SiliconPV 2024, 14th International Conference on Crystalline Silicon Photovoltaics
Advanced Manufacturing, Challenges for Industrial Devices
https://doi.org/10.52825/siliconpv.v2i.1291

Published: 06 Dec. 2024

# PECVD $Si_xC_y$ as Barrier Layer Against Aluminum in Solar Cells With poly-Si/$SiO_x$ Passivating Contacts

David Bäurle[1], Benjamin Gapp[1], Giso Hahn[1], Heiko Plagwitz[1], and Barbara Terheiden[1]

[1] University Konstanz, Germany

*Correspondence: David.baeurle@uni-konstanz.de

**Abstract.** We investigate the barrier properties of phosphorus-doped Si-rich silicon carbide ($Si_xC_y$) thin films deposited by PECVD against Al/Si alloying in the context of poly-Si/$SiO_x$ passivating contacts. The stability of the implied open circuit voltage ($iV_{OC}$) after firing of single-sided, full area screen-printed Al-contacts increases with carbon content of the barrier layer and depends on the crystallization scheme applied to the samples. Crystallized $Si_xC_y$ layers with an atomic C concentration of about 20 at.% deposited on pre-crystallized poly-Si predominantly show no significant decrease in $iV_{OC}$ values for peak firing temperatures up to 725°C.

**Keywords:** Passivating Contacts, Metallization, Aluminum, Silicon Carbide

## 1. Introduction

Solar cells with a passivating contact, based on poly-Si and a thin $SiO_x$ layer, show high efficiencies beyond η = 26% due to their excellent charge carrier selectivity and passivation quality under the metal contacts [1], [2]. Ag serves usually as contact metal. However, the availability of expensive materials as Ag becomes limiting for a terawatt scale production [3]. Therefore, alternatives to Ag are needed. Al metallization is such an approach. The drawback of Al in this context is the strong alloying with silicon that would dissolve the poly-Si/$SiO_x$ contact completely. The introduction of a barrier layer with sufficiently high conductivity between poly-Si and Al metallization is the solution investigated in this contribution. Different phosphorus-doped Si-rich $Si_xC_y$ thin films deposited by plasma-enhanced chemical vapour deposition (PECVD) are studied regarding their barrier properties against Al.

## 2. Experimental

For this work, n-type (42 and 18 Ωcm) Cz-Si wafers with a size of 156.75x156.75 $mm^2$ and a thickness of 150 µm were saw damage etched by KOH. Afterwards, the samples underwent wet chemical cleaning processes. A thin $SiO_x$ layer (~1.7 nm) was grown by thermal oxidation in a tube furnace. Subsequently, 100 nm of phosphorus-doped amorphous silicon ((n) a-Si) were deposited by PECVD. The samples were cut to a size of 50x50 $mm^2$ and subjected to different crystallization schemes, Figure 1. For samples of group A and B the (n) a-Si was pre-crystallized in a tube furnace at 920°C before 50 nm of amorphous phosphorus-doped PECVD (n) a-$Si_xC_y$ were deposited by using the precursors $SiH_4$, $CH_4$ and $PH_3$. A second temperature treatment at 920°C was applied to group B to additionally crystallize the (n) $Si_xC_y$ layer. Samples of group C were exposed to one combined crystallization step after depositing (n) a-$Si_xC_y$ onto the uncrystallized (n) a-Si. An overview of the crystallization schemes and sample composition is given in Figure 1.

To investigate the influence of the high temperature anneal on the $Si_xC_y$ layers we performed Fourier-transform infrared spectroscopy (FTIR) measurements to analyze the occurring bonds. Therefor we deposited the thin films on chemically polished FZ-Si.

The (n) a-$Si_xC_y$ deposition was carried out with varying $CH_4$ gas flow to adjust the carbon content whereas the other process conditions were kept constant. In the following the relation between $CH_4$ and $SiH_4$ gas flow ($R$) will be stated to identify the different samples. To quantify the carbon content, SIMS (secondary ion mass spectrometry) measurements were performed on selected samples.

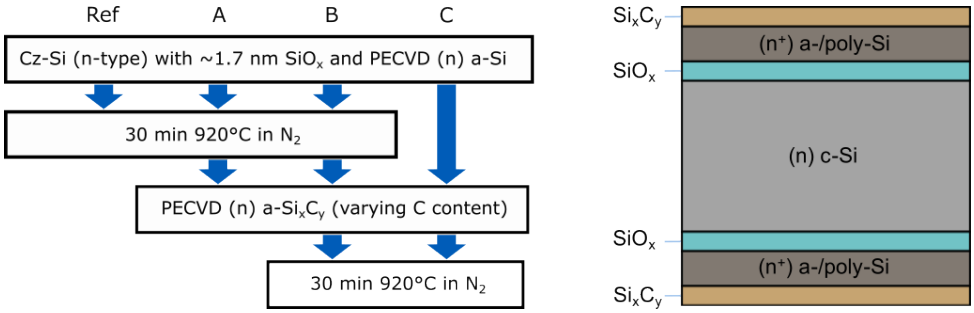


***Figure 1.*** *Process flow of the different crystallization schemes and the cross section of a typical sample.*

To examine the different barrier layers, the samples were single-sided full area screen-printed with Al-paste and fired in a conventional belt furnace. The measured peak temperatures, using a thermocouple, ranged between $T_{Peak}$ = 675-750°C with a measurement uncertainty of ±10°C.The barrier layer functionality was evaluated by comparing the $iV_{OC}$ values of the samples before screen-printing the Al-paste and after metallization and removal of Al in aqueous HCl. Photoconductance decay (PCD) measurements to determine $iV_{OC}$ were performed using a Sinton lifetime tester.

# 3. Results and Discussion

## 3.1 Crystallization schemes

The high temperature anneal leads to various changes in the $Si_xC_y$ thin films. Measurements with FTIR show that bonds are reorganized, Figure 2 (i). In the as-deposited a-$Si_xC_y$:H films Si-$H_n$ and C-$H_n$ bonds could be detected. The absorption band at 2070 $cm^{-1}$ can by assigned to the Si-$H_{1,2}$ stretching vibration [4]. Between 2800 $cm^{-1}$ and 3000 $cm^{-1}$ C-$H_n$ stretching vibrations cause weak absorption bands [5], [6]. In the crystallized $Si_xC_y$ films those hydrogen bonds are not detected anymore which indicates an effusion of hydrogen during the high temperature anneal. Si-C stretching vibrations lead to an absorption band between 760 $cm^{-1}$ and 800 $cm^{-1}$ [5], [6], [7]. In this range the absorption increases strongly after the crystallization which indicates that Si-C bonds are formed. An increasing absorption can also be observed around 1070 $cm^{-1}$. This can be assigned to various silicon and oxygen related bonds [8], [9]. Those Si-$O_x$ bonds are presumably formed at the surface, after the sample re-enters ambient air at a temperature of 800°C.

Another indication for this oxidation after crystallization can be seen in the glow-discharge optical emission spectroscopy (GD-OES) profiles of layer stacks processed after crystallization scheme B and C. In Figure 2 (ii), the profile of sample B shows an increased oxygen signal between the poly-Si and the $Si_xC_y$ layer which is not observed in sample C where no pre-crystallization of the a-Si was performed. The poly-Si can be identified between the onset of the carbon signal ($Si_xC_y$ layer) and the small oxygen signal at 13 s which corresponds to the thin interfacial $SiO_x$.

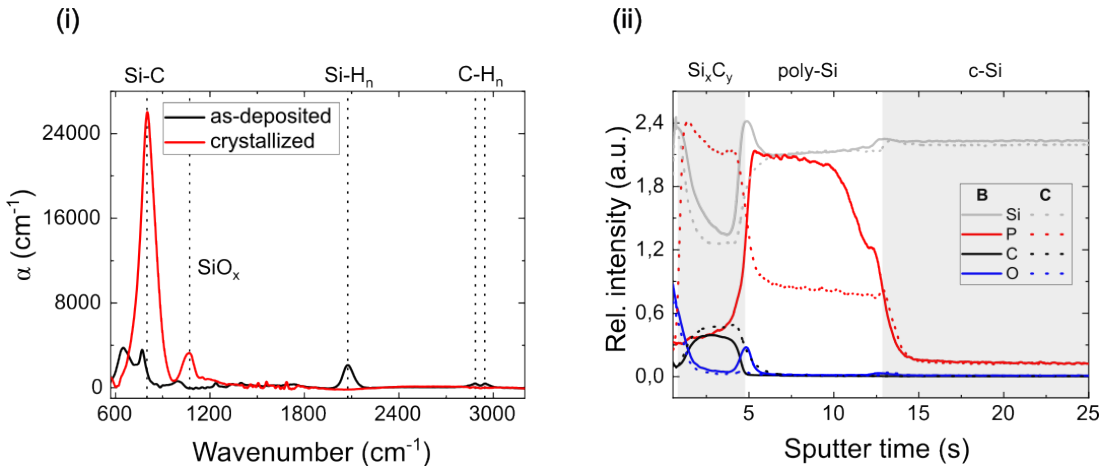


***Figure 2.*** (i) *Absorption spectrum of the $Si_xC_y$ layer before and after the high temperature anneal recorded via FTIR.* (ii) *GD-OES profile of samples crystallized after scheme B and C.*

The additionally arising $SiO_x$ in crystallization scheme B seems to be a diffusion barrier for the phosphorus in the poly-Si. In the sample with the additional $SiO_x$ the P signal in the poly-Si is significantly stronger than in the $Si_xC_y$ and c-Si. Whereas for the sample of group C the phosphorus seems to diffuse into the $Si_xC_y$ layer. Here the P signal is considerably higher in the $Si_xC_y$ layer than in the poly-Si.

Furthermore, it was analyzed how the crystallization scheme impacts the passivation quality. As seen in Figure 3, the initial $iV_{OC}$ values vary strongly with the applied sample preparation. Samples of group A show even without further hydrogenation an $iV_{OC}$ values up to 731 mV. The crystallization of the $Si_xC_y$ layers and the associated changes appear to deteriorate the surface passivation. In groups B and C, the initial $iV_{OC}$ values are limited to 698 mV or 685 mV respectively. If those samples are exposed to a hydrogenation by the deposition of an additional hydrogen-rich $SiN_x$ layer and a subsequent fast firing step, the passivation of groups B and C improve significantly. After hydrogenation all samples show excellent surface passivation with $iV_{OC}$ values in the range of 721-731 mV.

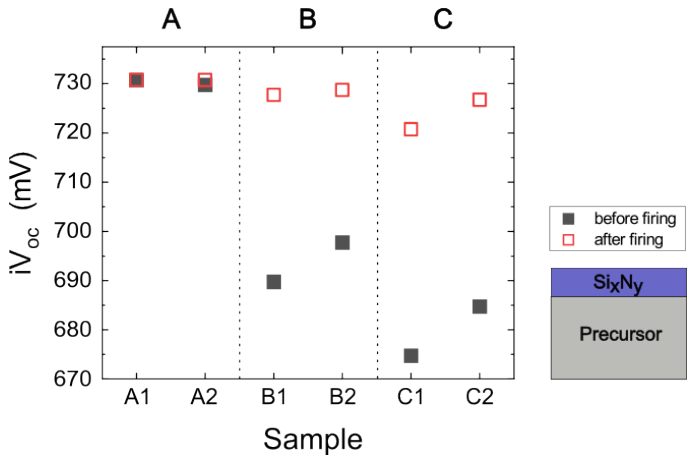


***Figure 3.*** *$iV_{OC}$ measurements of unmetallized samples processed after the different crystallization schemes before and after hydrogenation with $SiN_x$ and fast firing. The precursor shown in the schematic sample cross section equals the cross section illustrated in Figure 1.*

## 3.2 Barrier functionality

The influence of crystallization scheme and carbon content on the barrier functionality of $Si_xC_y$ layers is shown in Figure 4 (i) for samples of group A, B and C without hydrogenation. All represented samples were fired at a measured $T_{Peak}$ = 675°C. SIMS measurements indicate

that the carbon content for an increasing $R$ = 3-6 rises from around 10 to 20 at.%. Compared to the reference sample without barrier layer, samples of group A and B show significantly higher $iV_{OC}$ values after metallization and subsequent etch-back.

In particular, for samples with as-deposited barrier layers (group A) the carbon content seems to increase the stability of the $iV_{OC}$ after metallization. In Group A an initial $iV_{OC}$ up to 722 mV is achieved. After full-area metallization and etch-back, the $iV_{OC}$ of the sample with the a-$Si_xC_y$ layer with maximum carbon content is 711 mV. The loss in $iV_{OC}$ indicates a decreasing barrier functionality.

The second crystallization which is performed on samples of group B limits the initial $iV_{OC}$ to values of around 700 mV without hydrogenation. Nevertheless, those samples of group B show highest stability regarding $iV_{OC}$ after metallization with no shown decrease in the tested temperature range. As shown in the previous section, it is expected that an additional hydrogenation can overcome the limitation in the initial $iV_{OC}$. This makes the shown barrier functionality of group B most promising.

The combined crystallization of (n) a-Si and (n) a-$Si_xC_y$ applied in group C leads to samples with inferior barrier functionality. Only for the sample with highest carbon content the $iV_{OC}$ value after metallization and etch-back is higher than that of the reference sample without any barrier layer, shown in Figure 4 (i).

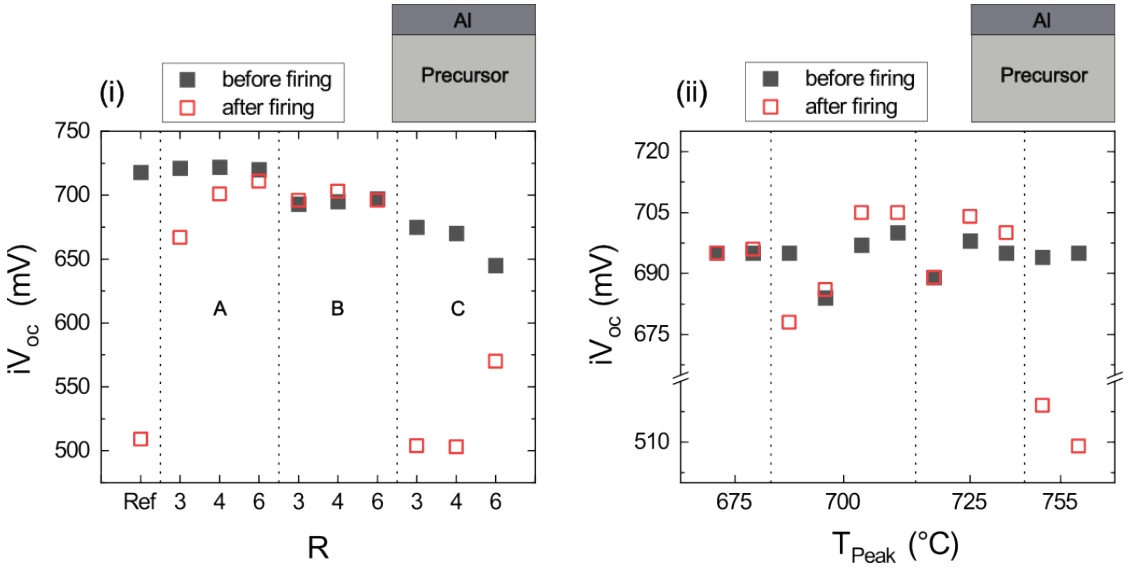


***Figure 4. (i)*** *$iV_{oc}$ measurements, before metallization and after metallization with subsequent etch-back, of samples (42 Ωcm) processed with varying crystallization scheme (A/B/C) and $CH_4/SiH_4$ ratio R fired at $T_{Peak}$ = 675°C.* ***(ii)*** *$iV_{oc}$ measurements, before metallization and after metallization with subsequent etch-back, of samples (18 Ωcm) with R = 6 and crystallization scheme B, fired at varying measured $T_{Peak}$. The precursor shown in the schematic sample cross sections equals the cross section illustrated in Figure 1.*

To further investigate the barrier functionality, a variation of the peak firing temperature was performed on samples which were crystallized following scheme B and featuring $Si_xC_y$ layers with maximum carbon content. The stability of $iV_{OC}$ values depending on $T_{Peak}$ is illustrated in Figure 4 (ii). Except for one sample the $iV_{OC}$ is not decreasing during metallization for temperatures up to $T_{Peak}$ = 725°C. The $iV_{OC}$ of some samples even shows a small increase of up to 8 mV. Firing the samples at $T_{Peak}$ = 755°C dissolves the poly-Si/$SiO_x$ passivating contact completely which results in $iV_{OC}$ values below 520 mV, which is comparable to the reference sample without barrier layer.

## 4. Conclusion

The ability of different PECVD $Si_xC_y$ layers to prevent aluminum from dissolving the poly-$Si/SiO_x$ passivating contact depends on both the crystallization scheme during sample preparation and the carbon content. The impact of the carbon content is mainly visible for samples with as-deposited barrier layers (group A). Here, the barrier functionality increases significantly with an increasing carbon content from 13.5(23) to 19.3(23) at.%. A pre-crystallization of the a-Si before depositing the $Si_xC_y$ seems to be even more important. Samples with one simultaneous crystallization (group C) show basically no barrier functionality compared to reference samples without barrier layer. Annealed $Si_xC_y$ layers which were deposited on pre-crystallized poly-Si (group B) exhibit the most promising barrier properties. For peak firing temperatures up to 725°C those sample show predominantly no decrease in $iV_{OC}$ after metallization with Al and subsequent Al removal.

## Data availability statement

The data that support the findings of this study are available from the corresponding author upon reasonable request.

## Author contributions

**D. Bäurle**: formal analysis, investigation, validation, visualization, conceptualization, writing – original draft; **B. Gapp**: conceptualization, validation; **G. Hahn**: supervision, writing – review & editing; **H. Plagwitz**: conceptualization, validation, supervision, project administration; **B. Terheiden**: conceptualization, supervision, funding acquisition, project administration, writing – review & editing

## Competing interests

The authors declare that they have no competing interests.

## Funding

Part of this work was financially supported by the German Federal Ministry for Economic Affairs and Climate Action (FKZ 03EE1106B). The content is the responsibility of the authors.

## Acknowledgement

The authors would like to thank Thomas Pernau for the a-Si depositions.

## References

[1] F. Haase, C. Hollemann, S. Schäfer, A. Merkle, M. Rienäcker, J. Krügener, R. Brendel, and R. Peibst, "Laser contact openings for local poly-Si-metal contacts enabling 26.1%-efficient POLO-IBC solar cells", Sol. Energy Mater. Sol. Cells, vol.186, pp. 184-193, Nov., 2018, doi: https://doi.org/10.1016/j.solmat.2018.06.020.

[2] A. Richter, R. Müller, J. Benick, F. Feldmann, B. Steinhauser, C. Reichel, A. Fell, M. Biv our, M. Hermle, and S. W. Glunz, "Design rules for high-efficiency both-sides-contacted silicon solar cells with balanced charge carrier transport and recombination losses", Nat. Energy, vol.6, no.4, pp. 429-438, Apr., 2021, doi: https://doi.org/10.1038/s41560-021-00805-w.

[3] Y. Zhang, M. Kim, L. Wang, P. Verlinden, and B. Hallam, "Design considerations for multi-terawatt scale manufacturing of existing and future photovoltaic technologies: challenges and opportunities related to silver, indium and bismuth consumption", Energy Environ. Sci., vol.14, no.11, pp. 5587-5610, Nov., 2021, doi: https://doi.org/10.1039/D1EE01814K.

[4] K.M. McNamara, B.E. Williams, K.K. Gleason, and B.E. Scruggs, "Identification of defects and impurities in chemical-vapor-deposited diamond through infrared spectroscopy", J. Appl. Phys., vol. 76, no. 4, Aug., 1994, doi: https://doi.org/10.1063/1.357598.

[5] P.I. Rovira, and F. Alvarez, "Chemical (dis)order in a-$Si_{1-x}C_x$:H for x<0.6", Phys. Rev. B, vol.55, no.7, pp. 4426-4434, Feb., 1997, doi: https://doi.org/10.1103/PhysRevB.55.4426.

[6] T. Friessnegg, M. Boudreau, P. Mascher, A. Knights, P.J. Simpson, and W. Puff, "Defect structure of carbon rich a-SiC:H films and the influence of gas and heat treatments", J. Appl. Phys., vol. 84, no. 2, Jul., 1998, doi: https://doi.org/10.1063/1.368138.

[7] N.V. Tzenov, M.B. Tzolov, and D.I. Dimova-Malinovska, "Hydrogen-assisted surface reactions during the growth of sputtered a-SiC:H films", Semicond. Sci. Technol., vol. 9, no. 1, pp. 91-96, Jan., 1994, doi: https://doi.org/10.1088/0268-1242/9/1/016.

[8] Z. An, R.K.Y. Fu, P. Chen, W. Liu, P.K. Chu, and C. Lin, "Silicon carbide formation by methane plasma immersion ion implantation into silicon", J. Vac. Sci. Technol. B, vol.21, no.4, pp. 1375-1379, Jul., 2003, doi: https://doi.org/10.1116/1.1591741.

[9] M. Künle, T. Kaltenbach, P. Löper, A. Hartel, S. Janz, O. Eibl, and K-G. Nickel, "Si-rich a-SiC:H thin films: Structural and optical transformations during thermal annealing", Thin Solid Films, vol.519, no.1, pp. 151-157, Oct., 2010, doi: https://doi.org/10.1016/j.tsf.2010.07.085.